Detection of cardiac amyloidosis with ^{18}F-Florbetaben-PET/CT in comparison to echocardiography, cardiac MRI and DPD-scintigraphy

Malte Kircher[1,2] · Sandra Ihne[2,3] · Joachim Brumberg[1] · Caroline Morbach[2,4] · Stefan Knop[3] · K. Martin Kortüm[3] · Stefan Störk[2,4] · Andreas K. Buck[1] · Theresa Reiter[4] · Wolfgang R. Bauer[4] · Constantin Lapa[1]

Abstract

Purpose Cardiac amyloidosis (CA) is a rare cause of heart failure with frequently delayed diagnosis, because specific early signs or symptoms are missing. Recently, direct amyloid imaging using positron emission tomography/computed tomography (PET/CT) has emerged.

The aim of this study was to examine the performance of ^{18}F-florbetaben-PET/CT in detection of CA, and compare it to echocardiography (echo), cardiac MRI (CMR) and scintigraphy. Additionally, the use of ^{18}F-florbetaben-PET/CT for quantification of amyloid burden and monitoring of treatment response was assessed.

Methods Twenty-two patients with proven ($n = 5$) or clinical suspicion ($n = 17$) of CA underwent ^{18}F-florbetaben-PET/CT for diagnostic work-up. Qualitative and quantitative assessment including calculation of myocardial tracer retention (MTR) was performed, and compared to echo ($n = 20$), CMR ($n = 16$), scintigraphy ($n = 16$) and serologic biomarkers (NT-proBNP, cTnT, free light chains). In four patients, follow-up PET/CT was available (after treatment initiation, $n = 3$; surveillance, $n = 1$).

Results PET demonstrated myocardial ^{18}F-florbetaben retention consistent with CA in 14/22 patients. Suspicion of CA was subsequently dropped in all eight PET-negative patients. Amyloid subtypes showed characteristic retention patterns (AL > AA > ATTR; all $p < 0.005$). MTR correlated with morphologic and functional parameters, as measured by CMR and echo (all $|r| > 0.47|$, all $p < 0.05$), but not with cardiac biomarkers. Changes in MTR from baseline to follow-up corresponded well to treatment response, as assessed by cardiac biomarkers and performance status.

Conclusions Imaging of cardiac amyloidosis (CA) with ^{18}F-florbetaben-PET/CT is feasible and might be useful in differentiating CA subtypes.

Keywords Amyloid imaging · Retention index · Response assessment · Diagnosis · Heart

Wolfgang R. Bauer and Constantin Lapa contributed equally to this work.

Electronic supplementary material The online version of this article (https://doi.org/10.1007/s00259-019-04290-y) contains supplementary material, which is available to authorized users.

✉ Theresa Reiter
Reiter_T@ukw.de

Malte Kircher
Kircher_M@ukw.de

[1] Department of Nuclear Medicine, University Hospital Würzburg, Oberdürrbacher Str. 6, 97078 Würzburg, Germany

[2] Comprehensive Heart Failure Center, University Hospital Würzburg, Würzburg, Germany

[3] Department of Internal Medicine II, Hemato-Oncology, University Hospital Würzburg, Würzburg, Germany

[4] Department of Internal Medicine I, Cardiology, University Hospital Würzburg, Oberdürrbacher Str. 6, 97078 Würzburg, Germany

Introduction

Amyloidosis is characterized by the pathologic, extracellular deposition of a variety of misfolded proteins as insoluble fibrils and can affect almost all organs. Out of the over 30 known subtypes of amyloidosis, light-chain (AL), transthyretin (ATTR) and secondary (AA) amyloidosis represent the clinically most relevant variants [1, 2].

Cardiac amyloidosis (CA) usually manifests as progressive heart failure with preserved ejection fraction due to restrictive cardiomyopathy, and is primarily caused by light chain (AL) and transthyretin (TTR) deposits [3, 4]. Since early clinical symptoms are uncharacteristic, CA is frequently misdiagnosed as hypertensive or hypertrophic cardiomyopathy. Only 40% of

patients are diagnosed within 6 months after onset of symptoms, and just 20% receive diagnosis after another latency of as long as three or more years [5].

Definite diagnosis of CA still requires histological proof of amyloid deposits on endomyocardial biopsy (EMB) [6], or, in patients with appropriate cardiac findings, of amyloid deposits on histologic examination of a biopsy from other tissues (e.g., abdominal fat pad, rectum, or kidney) [7, 8]. In experienced hands, sensitivity of EMB is high, but the technique is invasive, not unlimitedly repeatable and, due to an uneven distribution of amyloid deposits, does not provide reliable information on the actual amyloid burden for therapy monitoring [9].

Echocardiography (echo) is the standard of care method to assess cardiac dimensions and function. Typical findings of cardiac amyloidosis include increased wall thickness of the ventricles and interatrial septum, as well as signs of diastolic dysfunction. Although the detection rate of CA by echo was recently improved by introduction of speckle-tracking based stain imaging, with an amyloidosis-characteristic pattern of apical sparing, even advanced echocardiographic techniques still suffer from limited specificity [10, 11].

Cardiac magnetic resonance (CMR) imaging represents the gold standard for evaluation of morphological myocardial parameters with characteristic global, left-ventricular late gadolinium enhancement (LGE), resulting in sensitivities and specificities as high as 90% [12–14]. However, severe device artifacts due to pacemakers or implantable cardioverter defibrillators (ICD) can prevent adequate image interpretation. Moreover, impaired kidney function, which is highly prevalent in amyloidosis patients, prevents the use of contrast agents [15–17]. And although assessment of extracellular volume (ECV) by quantitative T1 mapping (either native or before and after application of contrast agent) has been reported as a promising biomarker for moderate micro-morphological changes, which presumably are present in early stages of the disease [18, 19], one would conjecture that molecular markers even precede these changes. Imaging of molecular markers is still the domain of nuclear techniques, and therefore suitable tracers are desirable.

Nuclear imaging, using scintigraphy with bone imaging agents such as ^{99m}Tc-labelled pyrophosphate or 3,3-diphosphono-1,2-propanodiacarboxylic acid (DPD), has proven a reliable tool for detection of TTR-type cardiac amyloidosis (in the absence of a monoclonal gammopathy) [20, 21]. However, direct visualization of amyloid burden (and treatment monitoring) in other subtypes such as AL or AA cannot be reliably performed. Likewise, the role of imaging with the most commonly used positron emission tomography (PET) tracer ^{18}F-FDG in this disease has not been established yet [22].

As an alternative, general feasibility of CA visualization by other PET tracers, using various direct amyloid imaging agents, could be demonstrated in first pilot studies [23–25]. One of these imaging agents is the fluorine-18-labeled stilbene derivate ^{18}F-florbetaben.

The aim of this study was to assess the performance of ^{18}F-florbetaben-PET/CT for detection of CA in comparison to the more established imaging modalities echo, CMR and scintigraphy. Additionally, the ability of ^{18}F-florbetaben-PET/CT to quantify amyloid burden for treatment response assessment was investigated.

Methods

Imaging was performed for diagnostic work-up or establishing the diagnosis of CA. All patients gave written informed consent prior to the investigations for receiving the respective imaging procedures. The study complied with the Declaration of Helsinki. Imaging data were retrospectively analyzed. A formal review for this retrospective analysis was waived by the ethics committee of the Universitätsklinikum Würzburg, Germany.

Subjects and study design

From March 2016 to August 2017, 22 patients (14 males and 8 females, mean age, 65 ± 14 years) with either direct histological evidence of CA by EMB ($n = 5$), or clinical suspicion of CA ($n = 17$), according to internationally accepted criteria (symptoms of heart failure, elevated cardiac biomarkers and otherwise histological evidence of amyloid [26, 27] as well as echocardiographic findings suggestive of amyloidosis), underwent imaging with ^{18}F-florbetaben-PET/CT (all), echo ($n = 20$), CMR ($n = 16$; 3 patients were excluded due to ICDs, 3 due to chronic kidney disease), as well as bone scintigraphy ($n = 16$). Median delay between PET/CT and other imaging modalities was 19 days (echo), 8 days (CMR) and 5 days (scintigraphy), respectively. Results of ^{18}F-florbetaben-PET/CT were compared to findings of echo, CMR and bone scintigraphy, respectively.

In four patients, follow-up PET/CT scans were available 6, 8, 11 and 15 months after initiation of therapy ($n = 3$) / surveillance ($n = 1$), respectively.

Detailed patient characteristics are given in Table 1 as well as in Tables S1–S3.

PET imaging

All PET scans were performed on a dedicated PET/CT scanner (Siemens Biograph mCT 64; Siemens, Erlangen, Germany). Injected activity ranged from 260 to 375 MBq (mean 313 ± 26 MBq). Cardiac imaging was dynamically performed, using 3D list mode, with the following set of time frames: ten frames of 10 s each, ten frames of 30 s each, ten frames of 60 s each and finally, three frames of 255 s each (total imaging duration

Table 1 Patient characteristics and imaging results

Patient data				Biomarkers		Imaging results				Underlying disease / final diagnosis	Location of biopsy
Patient number	Age (years)	Sex	Initial signs / symptoms & findings	NT-proBNP	cTnT	PET[a]	MTR	Scinti[b]	CMR		
1	78	Male	ECG, cardiac symptoms	5185	0.048	pos	41	pos	ICD	CA (ATTR)	None[c]
2	65	Male	ECG, MGUS	2764	0.017	pos	61	neg	pos	MGUS; CA (AL)	Abdominal fat, kidney
3	73	Male	ECG, MGUS	4824	0.047	pos	38	neg	ICD	MGUS; CA (AL)	Kidney
4	62	Male	TTE	1119	0.006	neg	24	neg	neg	LCDD, probably cardiac involvement	Kidney, liver
5	62	Male	AL-amyloidosis, dia. Dysfunction (TTE)	119	0.016	neg	33	neg	neg	Cutaneous AL-amyloidosis	Skin, gut (neg)
6	67	Female	TTE, AL-amyloidosis	409	0.143	neg	34	n/a	neg	Systemic AL-amyloidosis	Abdominal fat, kidney
7	75	Male	ECG	1176	0.026	pos	45	pos	pos	CA ($ATTR_{wt}$)	None[c]
8	78	Male	ECG, cardiac symptoms	3569	0.133	pos	42	pos	pos	CA (ATTR)	None[c]
9	73	Male	TTE, cardiac symptoms	*n/a*	0.005	neg	32	neg	neg	CAD, COPD	*n/a*
10	77	Female	TTE, AL-amyloidosis	6199	0.008	neg	31	neg	neg	MM; AL-amyloidosis and CAD	Mandibula, EMB (neg)
11	57	Female	AL-amyloidosis	10,785	0.025	pos	96	neg	pos	MM; CA (AL)	EMB
12	68	Female	cardiac symptoms, scintigraphy[d]	2246	0.023	pos	58	pos	CKD	Inflammatory active malignancy; CA (AA)	Gut, kidneys
13	57	Female	cardiac symptoms, AL-amyloidosis	5976	0.131	pos	111	n/a	pos	SMM, CA (AL)	Gut
14	68	Male	ECG, cardiac symptoms	1513	0.031	pos	38	pos	pos	CA ($ATTR_{wt}$)	EMB
15	61	Female	ECG, cardiac symptoms, SMM	77	0.013	pos	96	pos	pos	SMM; CA (AL)	EMB
16	68	Female	ECG, systemic AL-amyloidosis	339	0.010	neg	22	neg	neg	MM; systemic AL-amyloidosis	Colon
17	63	Male	AL-amyloidosis, rising cTNT/NT-pBNP	171	0.005	pos	62	n/a	neg	MGUS; potentially CA (AL)	Intestine
18	76	Male	ECG, cardiac symptoms, MM	1045	0.011	pos	70	n/a	ICD	MM; CA (AL)	EMB
19	67	Female	ECG, cardiac symptoms	4140	0.031	pos	45	pos	pos	CA ($ATTR_{wt}$)	None[c]
20	73	Male	ECG, MM	2012	0.038	pos	59	n/a	pos	MM; CA (AL)	Gastral
21	30	Male	ECG, AA-amyloidosis	excl.[e]	excl.[e]	neg	21	neg	CKD	Familial mediterranean fever; AA-amyloidosis	Kidney, gut
22	21	Male	TTE, Alport syndrome	excl.[e]	excl.[e]	neg	22	n/a	CKD	Hypertensive cardiomyopathy	None

[a] PET on visual inspection

[b] Scintigraphy on visual inspection

[c] Positive scintigraphy and excluded MGUS/MM

[d] Long-time patient with malignant paraganglioma without cardiac tracer-uptake in previous scintigraphic imaging

[e] Excluded due to distortions caused by chronic kidney failure/dialysis

$ATTR_{wt}$ transthyretin amyloidoisis of wild-type, *CAD* coronary artery disease, *CKD* chronic kidney disease, *CMR* cardiac MRI, *cTnT* cardiac Troponin T [in ng/ml], *ECG* electrocardiography, *EMB* endomyocardial biopsy, *FLC-diff* difference between involved and uninvolved free light chains [in mg/dl], *ICD* implantable cardioverter defibrillator, *MGUS* Monoclonal gammopathy of undetermined significance, *MM* Multiple myeloma, *NT-proBNP* N-terminal pro–B-type natriuretic peptide [in pg/ml], *MTR* Myocardial Tracer Retention [in %], *n/a* not applicable, *neg* negative, *pos* positive, *SMM* Smoldering multiple myeloma, *TTE* transthoracic echocardiography

approximately 30 min). All PET images were iteratively reconstructed (4 iterations, 12 subsets, matrix: 300 × 300, Gauss filtering: 5 mm), using dedicated manufacturer's software (syngo MI.PET/CT; Siemens Healthineers). The PET scanner is periodically checked for calibration accuracy as part of quality control according to published guidelines [28]. Low-dose CT of the thorax for attenuation correction was acquired (35 mAs, 120 keV, 512 × 512 matrix, 5 mm slice thickness, increment of 30 mm/s, rotation time of 0.5 s, and pitch of 0.8). For visual inspection, static images from PET data acquired

between 10 and 30 min after tracer injection were reconstructed. Images were analysed as previously described by Law et al. [25]: Percentage myocardial tracer retention (MTR, given in [%]) was calculated as the change in LV myocardial SUV_{mean} on summed-framed images of the first 5 min after i.v. injection of the tracer ($SUV_{0–5}$) and between 15 and 20 min ($SUV_{15–20}$), respectively, using the following formula as previously published:

$$MTR = \left[1-\left(\frac{SUV_{0–5}-SUV_{15–20}}{SUV_{0–5}}\right)\right]\cdot 100\%$$

The commercially available software PMOD, version 3.7 (PMOD Technologies LLC, Zuerich, Switzerland), was used for quantification of PET data. SUV_{mean} of the LV myocardium was measured by placing a VOI around the LV on summed-framed images of between 5 and 10 min after tracer-injection, using an automated iso-contouring threshold of 40% SUV_{max} as described [25].

Where available, ΔMTR, as the difference between follow-up and baseline percentage myocardial tracer retention indices, was calculated.

Echocardiography

Detailed echocardiography comprised an assessment of left and right ventricular dimensions and function, including global and regional longitudinal strain. For the assessment of diastolic function, we recorded early and late diastolic mitral inflow (E, A), as well as septal and lateral early diastolic myocardial relaxation velocity (e'). Features characteristic of amyloid were defined as the combined findings of thickened left ventricular walls (> 12 mm), impaired global strain (below −17%) with relative sparing of the apical region, and E/e' > 14, suggesting diastolic dysfunction. Presence of all parameters was required for diagnosis of CA.

CMR

CMR was performed on a 1.5 T (Achieva 1.5 T, Philips Healthcare, Best, The Netherlands) and 3.0 T (Achieva DS 3.0 T, Philips Healthcare, Best, The Netherlands) scanner. The protocol included a morphologic study based on balanced turbo field echo sequences for cine long- and short-axis views (field of view 380 mm, Flip angle 60°, TE 2.6–3.0 ms, TR 130–158 ms). Late enhancement imaging was performed 9–12 min after antecubital intravenous administration of 0.15 mmol/kg of a gadolinium-based contrast agent (Gadobutrol, Bayer HealthCare, Leverkusen, Germany). An inversion recovery T1 turbo field echo sequence was used, and the inversion time was adjusted to completely null the myocardial signal. Image analysis was performed, using the Extended Workspace software (EWS, Philips Healthcare, Best, The Netherlands), by two experienced cardiac CMR specialists (TR and WB). According to the Society for Cardiovascular Magnetic Resonance (SCMR) recommendations, cardiac morphology and function were analysed [29]. Late enhancement imaging was evaluated regarding global diffuse accumulation of contrast agent and very early nulling of the myocardium (less than 200 ms) in the look locker sequence, indicating amyloid affection. Functional and morphologic measurements were normalized to the body surface area (BSA). Findings rated typical of cardiac amyloidosis included (diffuse and heterogeneous) late gadolinium enhancement (LGE). At the time of our patient series, (quantitative) T1 mapping was not part of the routine protocol.

Scintigraphy

Whole-body planar scintigraphy was performed 3 h after intravenous injection of 488 to 700 MBq (mean 618 ± 31 MBq) of ^{99m}Tc-DPD. All images were acquired with a 20% energy window at 140 keV, using double head gamma cameras (Siemens Symbia; Siemens) equipped with low-energy, high-resolution collimators. Cardiac retention was analysed by two experienced readers (MK, CL), using the 4-point grading system recently described by Perugini et al. [30].

Serological biomarkers

For amyloidosis staging, according to the Revised Mayo Clinic Staging System ([31]; AL amyloidosis) and Grogan et al. ([32], ATTR), the cardiac and serologic biomarkers were measured on the day of PET imaging.

NT-proBNP and cTnT levels from one AA subject (patient #21), as well as one PET-negative subject (patient #22), were excluded from analysis because of distortions due to acute kidney failure/dialysis.

Statistical analysis

Statistical analyses were performed, using PASW Statistics software (version 22.0; SPSS, Inc. Chicago, IL). Quantitative values were expressed as mean ± standard deviation or median and range as appropriate. Comparisons of paired metric measurements were performed, using Wilcoxon-signed rank test. The chi square- or Fisher exact test was conducted for comparison of frequency data between independent subgroups. For bivariate correlation analyses, Spearman or Pearson correlation coefficients were calculated. Receiver operating characteristics were calculated for biomarker assessments to derive optimal thresholds for sensitivity and specificity, and respective AUCs were computed and compared. All statistical tests were performed two-sided and a p value <0.05 was considered to indicate statistical

significance. No correction for *p*-values was applied to adjust for multiple tests.

Results

Patient cohort and reference methods for the presence of amyloidosis

Twenty-two patients underwent ^{18}F-florbetaben-PET/CT for detection of cardiac amyloidosis. Systemic amyloidosis was finally proven in 19 patients by congo red positive biopsies and typing of amyloid (AL, $n = 12$; ATTR, $n = 5$; AA, $n = 2$; for location of biopsy see Table 1). In the remaining three patients, diagnosis of light chain deposition disease (LCDD; $n = 1$), Alport syndrome ($n = 1$) and coronary artery disease/chronic obstructive pulmonary disease ($n = 1$) were established, respectively.

The two patients in the AA subgroup suffered from malignant paraganglioma (patient #12), and familial Mediterranean fever (patient #21), respectively.

In the AL subgroup, multiple myeloma ($n = 5$), monoclonal gammopathy of unknown significance ($n = 3$) and smoldering multiple myeloma ($n = 2$) were most frequently associated with AL amyloidosis. NT-proBNP and cTnT were highly elevated with median values of 1529 pg/ml for NT-proBNP (range, 77–10,785 pg/ml) and 0.017 ng/ml for cTnT (range, 0.005–0.143 ng/ml), respectively, while median FLC-diff was 25 mg/dl (range, (−3)–2550 mg/dl).

In the ATTR subgroup ($n = 5$), median NT-proBNP levels amounted to 3569 pg/ml (range, 1176–5185 pg/ml) and median cTnT to 0.031 ng/ml (range, 0.026–0.133), respectively.

Individual patient data including disease stages according to current staging systems are shown in Tables S1 and S2.

PET results

On visual inspection, ^{18}F-florbetaben-PET/CT demonstrated moderate to intense myocardial tracer retention in 14/22 patients (8x AL, 5x ATTR; 1x AA). A relatively homogeneous ^{18}F-florbetaben distribution was observed in the myocardium of both ventricles and atria, proportional to the respective tissue volume. In 8/22 patients, no ^{18}F-florbetaben retention was observed. In these subjects, suspicion of CA was subsequently dropped due to normalization of cardiac biomarkers and unsuspicious follow-up echocardiography ($n = 4$), negative endomyocardial biopsy/myectomy ($n = 2$), diagnosis of non-amyloidogenic LCDD ($n = 1$), and diagnosis of hypertrophic cardiomyopathy ($n = 1$), respectively.

In semi-quantitative analysis, tracer retention was highest in patients suffering from AL-amyloidosis, followed by patients with AA- and TTR-amyloidosis, respectively (Fig. 1). CA patients with underlying AL-amyloidosis had a median MTR of 66 (range, 38–111), as compared to 42 (range, 38–45) in TTR-amyloidosis patients ($p < 0.01$). The PET-positive patient with AA-amyloidosis had a MTR of 58. Patients, in whom CA could finally be ruled out, had a median MTR of 27 (range, 21–34).

A MTR cut-off of ≤36 accurately separated CA from non-CA patients (sensitivity 100%, specificity 100%, AUC = 1.0, $p < 0.001$), with a cut-off of ≤52 differentiating between patients with TTR- and patients with type AA- and AL-amyloidosis, respectively (sensitivity 100%, specificity 89%, AUC = 0.91, $p < 0.005$). A cut-off of >59 separated patients with AL-amyloidosis from patients with other etiologies of CA (sensitivity 88%, specificity 100%, AUC = 0.96, $p < 0.001$). More detailed tracer kinetics of the different CA subtypes are shown in Figure S1.

Comparison to echocardiography

Comparing PET to echocardiography, MTR showed correlations to left ventricle wall thickness ($r = 0.46$, $p < 0.05$), and apical sparing of the longitudinal strain pattern ($r = 0.52$, $p < 0.02$), respectively. MTR also correlated to E/e' as a parameter of diastolic dysfunction ($r = 0.52$, $p < 0.02$). We found a negative correlation of MTR to tricuspid annular plane systolic excursion ($r = -0.50$, $p < 0.03$) and a trend to negatively correlate to mitral annular plane systolic excursion ($r = -0.43$, $p < 0.06$), respectively. Furthermore, MTR had a negative correlation to left ventricular end-diastolic volume ($r = -0.49$, $p < 0.03$).

Comparison to CMR

Overall concordance to CMR was 13/14 PET-positive patients (94%) with comparable results regarding the extent of affected myocardium. There was one PET-positive patient that showed no abnormalities in CMR. All patients without myocardial tracer retention showed concordant physiologic results in CMR (8/8). MTR significantly correlated with left ventricle (LV) lateral wall thickness ($r = 0.51$, $p < 0.05$) and tended to correlate with septal wall thickness ($r = 0.44$, $p < 0.09$). MTR correlated negatively with stroke index ($r = -0.60$, $p < 0.02$).

Comparison to scintigraphy

Findings of PET and scintigraphy matched in 81% of patients (7/10 positive, 6/6 negative), with all ATTR patients showing intense myocardial tracer-uptake in scintigraphy (score 3). One patient with AA amyloidosis showed mild to moderate (score 1) and one patient with AL amyloidosis intense myocardial uptake (score 3),

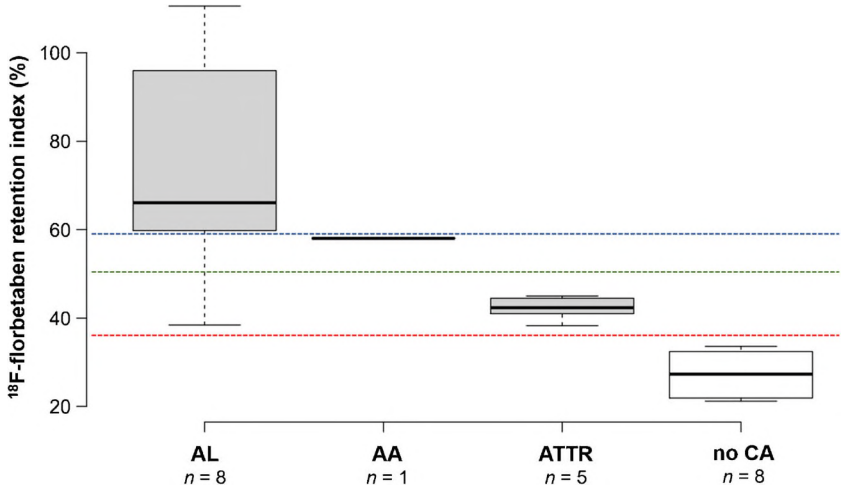

Fig. 1 Boxplot of percentage myocardial ^{18}F-florbetaben retention for CA subtypes Notes: no CA = no cardiac amyloidosis; A MTR cut-off of ≤36 (*red dotted line*) accurately separated patients with CA from patients without CA, respectively (sensitivity 100%, specificity 100%, $p < 0.001$). A cut-off of ≤52 (*green dotted line*) could differentiate between patients with TTR- and patients with type AA- and AL-amyloidosis, respectively (sensitivity 100%, specificity 89%, $p < 0.005$). A MTR cut-off of >59 (*blue dotted line*) separated patients with AL-amyloidosis from patients with other etiologies of CA (sensitivity 88%, specificity 100%, $p < 0.001$)

respectively. All other patients with AL amyloidosis showed no myocardial tracer-uptake (score 0). MTR did not correlate with intensity of tracer-uptake according to the Perugini scoring system (Fig. 2).

Comparison to serum biomarkers

MTR showed no correlation with cardiac biomarkers and free-light chain measurements (in case of type AL amyloidosis). Particularly cTNT (r = 0.13, $p = 0.60$), NT-proBNP (r = 0.27, $p = 0.26$) and FLC-diff, in case of AL amyloidosis (r = −0.11, $p = 0.80$), did not correlate with myocardial MTR.

Neither did MTR correlate to disease stage, as assessed by the Revised Mayo Clinic Staging System ([31]; type AL) and Grogan et al. ([32]; type ATTR), respectively.

Follow-up

Follow-up PET imaging was performed in four patients, after anti-amyloid treatment initiation ($n = 3$) or surveillance ($n = 1$), respectively.

The first follow-up patient (#11, type AL) with initially high MTR (96) demonstrated even higher retention at follow-up (119), after 6 months of treatment with bortezomib / prednisone. This observation conflicted with decreasing NT-proBNP, cTnT, and FLC-diff levels, but corresponded well with development of progressive heart failure, necessitating subsequent heart transplantation.

The second follow-up patient (#12, type AA) was staged about 8 months after initiation of *off-label* treatment with tocilizumab, an interleukin-6-receptor blocker. PET-derived MTR dropped from 58 at baseline to 29 at follow-up, corresponding well with a drop in cardiac markers, in serum amyloid A (SAA) as well as with improved clinical performance status (NYHA II-III at baseline, NYHA I at follow-up).

In the third follow-up patient (#17, type AL) re-staging was performed after surveillance of 15 months. MTR rose from 62 at baseline to 80 at follow-up, corresponding to a concomitant rise of cardiac biomarkers as well as FLC-diff.

The last follow-up patient (#19, type $ATTR_{wt}$) was staged 11 months after initiation of *off-label* treatment with tafamidis, a transthyretin-stabilizer approved for treatment of amyloid polyneuropathy due to TTR-amyloidosis. MTR remained generally stable with 45 at baseline as compared to 39 at follow-up, corresponding to unchanged cardiac symptoms and clinical findings.

Details on the follow-up patients can be found in Table S3.

Discussion

This study evaluated the performance of PET imaging of cardiac amyloidosis with ^{18}F-florbetaben in comparison to the more established imaging modalities of echocardiography, CMR and (bone) scintigraphy. Cardiac involvement was identified both visually, and by fully-automated quantitative analysis, including calculation of myocardial tracer retention.

Amyloid subtypes show characteristic patterns of tracer retention

^{18}F-florbetaben-PET/CT demonstrated its ability to differentiate three different subtypes of CA (AL, ATTR, AA). In line with previous results [23, 25], CA of AL-type displayed significantly higher tracer retention as

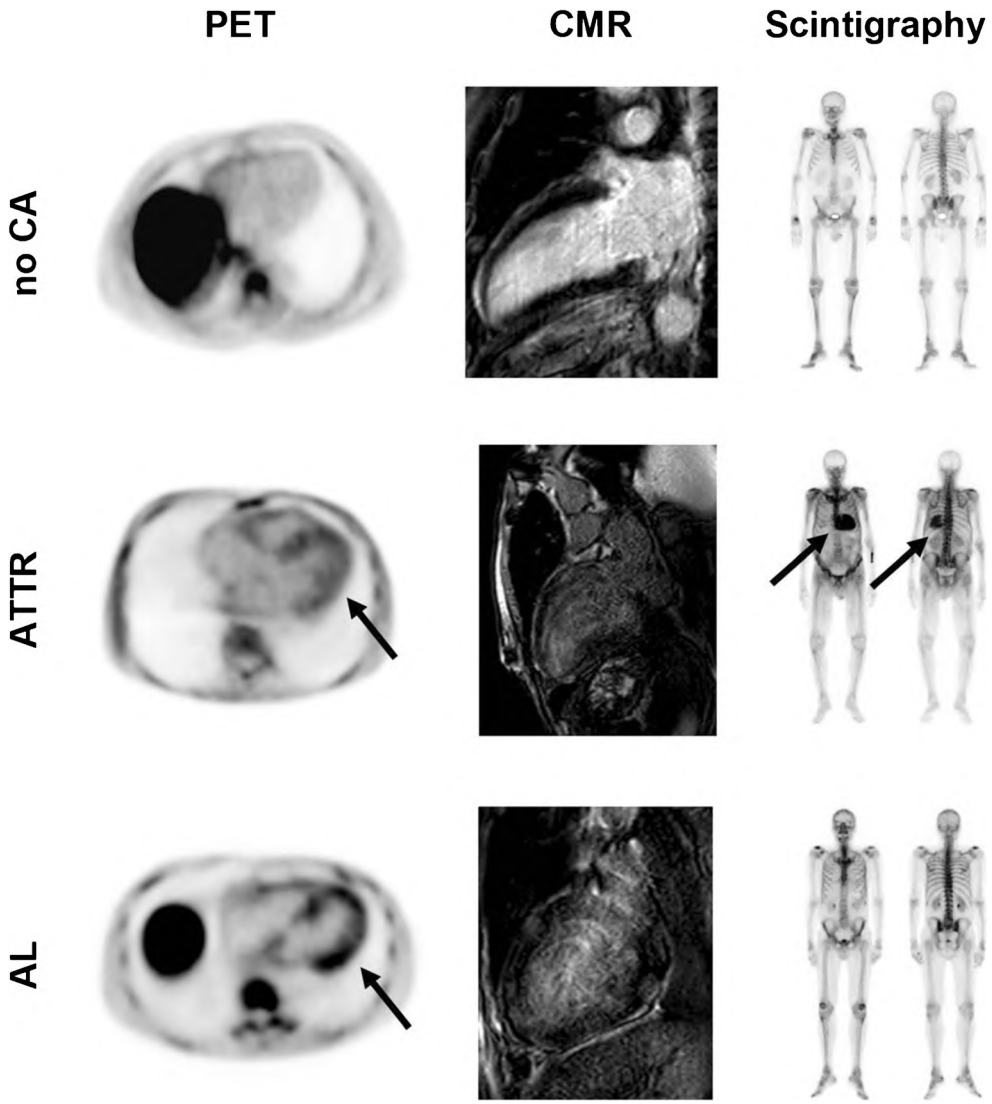

Fig. 2 Case examples Notes: PET = Positron emission tomography with ^{18}F-florbetaben; CMR = T1-weighted late gadolinium enhanced cardiac magnetic resonance imaging; Scintigraphy = whole body planar scintigraphy 3 h after i.v. injection of ^{99m}Tc-DPD; AL = light chain amyloidosis; ATTR = transthyretin amyloidosis; No CA = no cardiac amyloidosis; arrows = myocardial tracer accumulation. Upper row (No CA) = patient # 4, no cardiac tracer retention in PET/scintigraphy, normal CMR. Middle row (ATTR) = patient # 8, moderate cardiac tracer retention in PET (*arrow*; percentage myocardial retention: 42), diffuse global fibrosis in CMR and intense cardiac tracer retention in scintigraphy (*arrows*). Lower row (AL) = patient # 2, intense cardiac tracer retention in PET (*arrow*; percentage myocardial retention: 61), diffuse global fibrosis in CMR but no tracer retention in scintigraphy

compared with TTR-type CA. Noteworthy, the only CA patient in the AL subgroup with MTR < 59 (38) was being treated with bortezomib at the time of PET imaging, and the rather low MTR might reflect organ response. The MTR for the only subject with AA-type CA was between the other two CA types. To our knowledge this is the first time AA-type CA was visualized by ^{18}F-florbetaben-PET/CT, so no conclusions can be drawn.

In this pilot study, the MTR cut-off to separate CA from non-CA patients was well in line with the value published by Law et al. (our cohort, 36; sensitivity 100%, specificity 100%; Law et al., 40). Additionally, ^{18}F-florbetaben-PET seemed to distinguish between the underlying amyloid types with MTR > 36 and ≤ 51.5 for ATTR (sensitivity 100%, specificity 89%) and > 58.5 for AL (sensitivity of 88%, specificity of 100%), respectively. However, given the small sample size and the overlap between the AL and ATTR groups in the current cohort, further larger trials investigating the performance of ^{18}F-florbetaben-PET for amyloid type distinction are needed.

PET visualizes the molecular correlate of morphologic- and functional myocardial changes, as assessed by CMR and echo

Compared with the different imaging modalities (echo, CMR), PET-derived MTR showed remarkable correlations with both morphologic (LV wall thickness, relative apical sparing of the longitudinal strain pattern), and functional (E/e', TAPSE, LVEDV, stroke index) parameters of CA, thus strengthening the hypothesis of ^{18}F-florbetaben-PET's utility as a tool for non-invasive read-out of the underlying molecular amyloid burden, especially in patients who cannot undergo CMR due to ICDs or (amyloid-related) renal impairment.

PET might assist in accurate disease staging in patients with impaired kidney function

We could not demonstrate any correlation between tracer retention and cardiac biomarkers, or FLC-diff (in case of AL amyloidosis), respectively. Discordant results of serum parameters and imaging were highlighted in a patient (#11, AL amyloidosis) with treatment-induced improvement of serological parameters (Table S3), but increasing ^{18}F-florbetaben retention at follow-up, corresponding well with progressive heart failure and the need for heart transplantation. The failure to accurately estimate disease burden with these biomarkers might be partially explained by their dependence on kidney function on the one hand, and a decrease in NT-proBNP by adequate heart failure pharmacotherapy, despite progression of the underlying disease, on the other hand. Although no firm conclusions can be drawn from this pilot study, ^{18}F-florbetaben-PET might more accurately identify amyloid burden in respective cases.

Amyloid quantification for therapy response assessment

Amyloid-directed PET might also prove useful in (semi-quantitative) assessment of therapy response: For the first time we present data of follow-up imaging, after treatment initiation with anti-inflammatory (AA), anti-myeloma (AL) and TTR-stabilizing (ATTR) therapies, respectively. Quantification of amyloid burden, as expressed by MTR and ΔMTR, corresponded with changes in performance status and serological markers (Table S3).

^{18}F-florbetaben-PET for early detection of CA

Early diagnosis of CA is paramount, as median survival from onset of heart failure is less than a year and timely commencement of treatment can considerably extend life, particularly in case of type AL CA. Molecular imaging techniques may be able to identify CA at a very early stage and even earlier than CMR techniques. Therefore, the follow-up of the only patient (#17, AL amyloidosis) with discordant imaging results at baseline is noteworthy. While both CMR and echo were unremarkable, ^{18}F-florbetaben-PET indicated myocardial disease involvement. Over the ensuing 15 months, cardiac biomarkers and NYHA class progressively deteriorated, consistent with developing heart failure. Follow-up PET demonstrated a higher MTR, as compared to baseline (80 to 62, Table S3). Since no histologic proof of CA could be obtained (due to the patient's refusal to undergo EMB), it can only be speculated that this patient suffered from CA.

Limitations

Our study has various limitations. Firstly, the patient cohort was small and heterogeneous, including treatment-naïve, as well as pre-treated patients, with different underlying etiologies. Thus, all conclusions must be drawn with caution. In most patients, histologic proof of cardiac involvement could not be obtained. Additionally, although high sensitivity and specificity for the detection of amyloid β-plaques by ^{18}F-florbetaben-PET in Alzheimer's disease has been demonstrated, direct histologic proof for the detection of different CA subtypes by PET has not been provided yet.

No histological work-up of ^{18}F-florbetaben binding to cardiac amyloid, to further analyze therapy-induced changes in MTR, could be performed. However, to really assess the potential of amyloid-directed PET as a non-invasive instrument of (early) therapy monitoring, an understanding of the underlying biology is of utmost importance.

Moreover, since this pilot study focused on cardiac involvement, the value of additional whole-body imaging, to detect further sites of organ involvement in systemic amyloidosis, was not performed but should be addressed in future studies.

Finally, quantitative CMR imaging including determination of ECV by T1 mapping before and after application of contrast agent or sole native T1 mapping [18, 19] was not systematically performed as it was not routinely established at the time of the study. Follow-up trials enrolling larger numbers of patients should include quantitative CMR techniques for both early diagnosis of amyloidosis as well as therapy monitoring to allow for comparison to ^{18}F-florbetaben-PET/CT.

Conclusion

Imaging of cardiac amyloidosis (CA) with ^{18}F-florbetaben-PET/CT is feasible and might be useful in differentiating CA subtypes, irrespective of their underlying etiology. ^{18}F-florbetaben-PET/CT might prove a valuable new tool for quantification of amyloid burden. Based on these pilot data, further studies investigating its suitability for treatment response assessment in patients undergoing anti-amyloid therapy are highly warranted.

Acknowledgments We thank all people involved in this project, particularly our colleagues from the departments of cardiology and haematology, who left no stone unturned when caring for and treating our common patients.

Compliance with ethical standards

Ethical approval All procedures involving human participants were in accordance with the ethical standards of the institutional and/or national research committee and with the 1964 Helsinki declaration and its later amendments or comparable ethical standards.

Informed consent Informed consent was obtained from all individual participants included in the study.

Conflict of interest All authors state that they have nothing to disclose.

Publisher's note Springer Nature remains neutral with regard to jurisdictional claims in published maps and institutional affiliations.

References

1. Falk RH, Comenzo RL, Skinner M. The systemic amyloidoses. N Engl J Med. 1997;337:898–909. https://doi.org/10.1056/NEJM199709253371306.
2. Merlini G, Bellotti V. Molecular mechanisms of amyloidosis. N Engl J Med. 2003;349:583–96. https://doi.org/10.1056/NEJMra023144.
3. Alexander KM, Singh A, Falk RH. Novel pharmacotherapies for cardiac amyloidosis. Pharmacol Ther. 2017;180:129-138. https://doi.org/10.1016/j.pharmthera.2017.06.011.
4. Falk RH. Cardiac amyloidosis: a treatable disease, often overlooked. Circulation. 2011;124:1079–85. https://doi.org/10.1161/CIRCULATIONAHA.110.010447.
5. Lousada I, Comenzo RL, Landau H, Guthrie S, Merlini G. Light chain amyloidosis: patient experience survey from the amyloidosis research consortium. Adv Ther. 2015;32:920–8. https://doi.org/10.1007/s12325-015-0250-0.
6. Gertz MA, Lacy MQ, Dispenzieri A, Hayman SR. Amyloidosis: diagnosis and management. Clin Lymphoma Myeloma. 2005;6:208–19. https://doi.org/10.3816/CLM.2005.n.048.
7. Fernandez de Larrea C, Verga L, Morbini P, Klersy C, Lavatelli F, Foli A, et al. A practical approach to the diagnosis of systemic amyloidoses. Blood. 2015;125:2239–44. https://doi.org/10.1182/blood-2014-11-609883.
8. Foli A, Palladini G, Caporali R, Verga L, Morbini P, Obici L, et al. The role of minor salivary gland biopsy in the diagnosis of systemic amyloidosis: results of a prospective study in 62 patients. Amyloid. 2011;18(Suppl 1):80–2. https://doi.org/10.3109/13506129.2011.574354029.
9. Kristen AV, Dengler TJ, Katus HA. Suspected cardiac amyloidosis: endomyocardial biopsy remains the diagnostic gold-standard. Am J Hematol. 2007;82:328. https://doi.org/10.1002/ajh.20745.
10. Phelan D, Collier P, Thavendiranathan P, Popovic ZB, Hanna M, Plana JC, et al. Relative apical sparing of longitudinal strain using two-dimensional speckle-tracking echocardiography is both sensitive and specific for the diagnosis of cardiac amyloidosis. Heart. 2012;98:1442–8. https://doi.org/10.1136/heartjnl-2012-302353.
11. Liu D, Hu K, Niemann M, Herrmann S, Cikes M, Stork S, et al. Effect of combined systolic and diastolic functional parameter assessment for differentiation of cardiac amyloidosis from other causes of concentric left ventricular hypertrophy. Circ Cardiovasc Imaging. 2013;6:1066–72. https://doi.org/10.1161/CIRCIMAGING.113.000683.
12. Syed IS, Glockner JF, Feng D, Araoz PA, Martinez MW, Edwards WD, et al. Role of cardiac magnetic resonance imaging in the detection of cardiac amyloidosis. JACC Cardiovasc Imaging. 2010;3:155–64. https://doi.org/10.1016/j.jcmg.2009.09.023.
13. Ruberg FL, Appelbaum E, Davidoff R, Ozonoff A, Kissinger KV, Harrigan C, et al. Diagnostic and prognostic utility of cardiovascular magnetic resonance imaging in light-chain cardiac amyloidosis. Am J Cardiol. 2009;103:544–9. https://doi.org/10.1016/j.amjcard.2008.09.105.
14. Austin BA, Tang WH, Rodriguez ER, Tan C, Flamm SD, Taylor DO, et al. Delayed hyper-enhancement magnetic resonance imaging provides incremental diagnostic and prognostic utility in suspected cardiac amyloidosis. JACC Cardiovasc Imaging. 2009;2:1369–77. https://doi.org/10.1016/j.jcmg.2009.08.008.
15. Reiter T, Ritter O, Prince MR, Nordbeck P, Wanner C, Nagel E, et al. Minimizing risk of nephrogenic systemic fibrosis in cardiovascular magnetic resonance. J Cardiovasc Magn Reson. 2012;14:31. https://doi.org/10.1186/1532-429X-14-31.
16. Sommer T, Bauer W, Fischbach K, Kolb C, Luechinger R, Wiegand U, et al. MR imaging in patients with cardiac pacemakers and implantable cardioverter defibrillators. Rofo. 2017;189:204–17. https://doi.org/10.1055/s-0043-102029.
17. Falk RH, Quarta CC, Dorbala S. How to image cardiac amyloidosis. Circ Cardiovasc Imaging. 2014;7:552–62. https://doi.org/10.1161/CIRCIMAGING.113.001396.
18. Haaf P, Garg P, Messroghli DR, Broadbent DA, Greenwood JP, Plein S. Cardiac T1 mapping and extracellular volume (ECV) in clinical practice: a comprehensive review. J Cardiovasc Magn Reson. 2016;18:89. https://doi.org/10.1186/s12968-016-0308-4.
19. Martinez-Naharro A, Kotecha T, Norrington K, Boldrini M, Rezk T, Quarta C, et al. Native T1 and extracellular volume in transthyretin amyloidosis. JACC Cardiovasc Imaging. 2018. https://doi.org/10.1016/j.jcmg.2018.02.006.
20. Gillmore JD, Maurer MS, Falk RH, Merlini G, Damy T, Dispenzieri A, et al. Nonbiopsy diagnosis of cardiac transthyretin amyloidosis. Circulation. 2016;133:2404–12. https://doi.org/10.1161/CIRCULATIONAHA.116.021612.
21. Dorbala S, Bokhari S, Miller EJ, Bullock-Palmer R, Soman P, Thompson RE, et al. 99mTechnetium-pyrophosphate imaging for transthyretin cardiac amyloidosis. ASNC Pract Points, 2016.
22. Mekinian A, Jaccard A, Soussan M, Launay D, Berthier S, Federici L, et al. 18F-FDG PET/CT in patients with amyloid light-chain amyloidosis: case-series and literature review. Amyloid. 2012;19:94–8. https://doi.org/10.3109/13506129.2012.682833.
23. Dorbala S, Vangala D, Semer J, Strader C, Bruyere JR Jr, Di Carli MF, et al. Imaging cardiac amyloidosis: a pilot study using (1)(8)F-florbetapir positron emission tomography. Eur J Nucl Med Mol Imaging. 2014;41:1652–62. https://doi.org/10.1007/s00259-014-2787-6.
24. Antoni G, Lubberink M, Estrada S, Axelsson J, Carlson K, Lindsjo L, et al. In vivo visualization of amyloid deposits in the heart with 11C-PIB and PET. J Nucl Med. 2013;54:213–20. https://doi.org/10.2967/jnumed.111.102053.
25. Law WP, Wang WY, Moore PT, Mollee PN, Ng AC. Cardiac amyloid imaging with 18F-Florbetaben PET: a pilot study. J Nucl Med. 2016;57:1733–9. https://doi.org/10.2967/jnumed.115.169870.
26. Palladini G, Merlini G. What is new in diagnosis and management of light chain amyloidosis? Blood. 2016;128:159–68. https://doi.org/10.1182/blood-2016-01-629790.
27. Gertz MA, Comenzo R, Falk RH, Fermand JP, Hazenberg BP, Hawkins PN, et al. Definition of organ involvement and treatment response in immunoglobulin light chain amyloidosis (AL): a consensus opinion from the 10th international symposium on amyloid and amyloidosis, Tours, France, 18-22 April 2004. Am J Hematol. 2005;79:319–28. https://doi.org/10.1002/ajh.20381.
28. Boellaard R. Need for standardization of 18F-FDG PET/CT for treatment response assessments. J Nucl Med. 2011;52(Suppl 2):93S–100S. https://doi.org/10.2967/jnumed.110.085662.

29. Schulz-Menger J, Bluemke DA, Bremerich J, Flamm SD, Fogel MA, Friedrich MG, et al. Standardized image interpretation and post processing in cardiovascular magnetic resonance: Society for Cardiovascular Magnetic Resonance (SCMR) board of trustees task force on standardized post processing. J Cardiovasc Magn Reson. 2013;15:35. https://doi.org/10.1186/1532-429X-15-35.
30. Perugini E, Guidalotti PL, Salvi F, Cooke RM, Pettinato C, Riva L, et al. Noninvasive etiologic diagnosis of cardiac amyloidosis using 99mTc-3,3-diphosphono-1,2-propanodicarboxylic acid scintigraphy. J Am Coll Cardiol. 2005;46:1076–84. https://doi.org/10.1016/j.jacc.2005.05.073.
31. Kumar S, Dispenzieri A, Lacy MQ, Hayman SR, Buadi FK, Colby C, et al. Revised prognostic staging system for light chain amyloidosis incorporating cardiac biomarkers and serum free light chain measurements. J Clin Oncol. 2012;30:989–95. https://doi.org/10.1200/JCO.2011.38.5724.
32. Grogan M, Scott CG, Kyle RA, Zeldenrust SR, Gertz MA, Lin G, et al. Natural history of wild-type transthyretin cardiac amyloidosis and risk stratification using a novel staging system. J Am Coll Cardiol. 2016;68:1014–20. https://doi.org/10.1016/j.jacc.2016.06.033.